Earth and Planetary Science Letters 269 (2008) 259–270

Contents lists available at ScienceDirect

Earth and Planetary Science Letters

journal homepage: www.elsevier.com/locate/epsl

Thermally induced brittle deformation in oceanic lithosphere and the spacing of fracture zones

Eun-seo Choi *, Michael Gurnis

Seismological Laboratory, California Institute of Technology, Pasadena, CA 91125 U.S.A

ARTICLE INFO

Article history:
Received 22 June 2007
Received in revised form 24 January 2008
Accepted 8 February 2008
Available online 29 February 2008
Editor: C.P. Jaupart

Keywords:
oceanic lithosphere
fracture zone
thermal stress
brittle deformation

ABSTRACT

Brittle deformation of oceanic lithosphere due to thermal stress is explored with a numerical model, with an emphasis on the spacing of fracture zones. Brittle deformation is represented by localized plastic strain within a material having an elasto-visco-plastic rheology with strain softening. We show that crustal thickness, creep strength, and the rule governing plastic flow control the formation of cracks. The spacing of primary crack decreases with crustal thickness as long as it is smaller than a threshold value. Creep strength shifts the threshold such that crust with strong creep strength develops primary cracks regardless of crustal thicknesses, while only a thin crust can have primary cracks if its creep strength is low. For a thin crust, the spacing of primary cracks is inversely proportional to the creep strength, suggesting that creep strength might independently contribute to the degree of brittle deformation. Through finite versus zero dilatation in plastic strain, associated and non-associated flow rule results in nearly vertical and V-shaped cracks, respectively. Changes in the tectonic environment of a ridge system can be reflected in variation in crustal thickness, and thus related to brittle deformation. The fracture zone-free Reykjanes ridge is known to have a uniformly thick crust. The Australian-Antarctic Discordance has multiple fracture zones and thin crust. These syntheses are consistent with enhanced brittle deformation of oceanic lithosphere when the crust is thin and *vice versa*.

1. Introduction

The length of the mid-ocean ridge segments varies substantially among spreading centers and is correlated with several tectonic factors, including a positive correlation with spreading rate. The first order segments, bounded by transform faults (first order discontinuities), have an average length of 600±300 km along fast (>6 cm/yr) spreading ridges and 400±200 km for slow (<6 cm/yr) spreading ridges (MacDonald et al., 1991). Sandwell (1986) suggested that the length of the first order segments varies linearly with spreading rates. Although valid at the first order scale, such linear correlations are not supported at every level of the hierarchy. For example, the magmatic segments of slow to intermediate spreading ridges were shown to be 52.5 km long on average, independent of spreading rates (Briais and Rabinowicz, 2002).

Segment lengths are also apparently associated with regional variations in crustal thickness, creep strength, and mantle temperature. For instance, the Reykjanes ridge above the Iceland hot spot is known to have a uniform and much thicker crust for its spreading rate (Bunch and Kennett, 1980; Murton and Parson, 1993; Smallwood and White, 1998). This hot spot-affected ridge has been shown to exhibit signatures of wet mantle source for basaltic melt (Nichols et al., 2002). The water in crustal and mantle minerals has a strong weakening effect on creep strength although the preferential partitioning of water into melt phases complicates this straightforward relation (e.g., Karato, 1986; Hirth and Kohlstedt, 1996). In contrast, the Australian-Antarctic Discordance (AAD) has a highly rugged seafloor indicating increased fracturing (Hayes and Conolly, 1972; Weissel and Hayes, 1974) as well as anomalously thinner crust in comparison with other parts of the Southeast Indian Ridge (SEIR) (Tolstoy et al., 1995; Okino et al., 2004). Such regional features were attributed to colder mantle beneath the AAD (Weissel and Hayes, 1974), a hypothesis that was later supported by the systematics of major elements of basalt along the SEIR (Klein et al., 1991). These two regions, the Reykjanes ridge and the AAD, respectively exhibit reduced and enhanced segmentations at both the 1st and 2nd order compared with the other parts of the respective ridge systems. The degree of fracturing in those regions is substantially different in the profiles of free-air gravity anomaly (Fig. 1). The profile for the Reykjanes ridge (A–A') is smooth over the segment closer to Iceland and becomes rugged towards the southern end. The profile B–B' along the SEIR shows strong high frequency changes in depth and free-air gravity associated with the fracture zones over the AAD and with abrupt transition to a smooth segment east of the AAD.

A magma supply model has been proposed to explain the fundamentally different characteristics between slow- and fast-spreading centers, as well as axial morphology of a single ridge segment.

* Corresponding author. Tel.: +1 626 395 6971; fax: +1 626 564 0715.
E-mail address: ces74@gps.caltech.edu (E. Choi).

0012-821X/$ – see front matter © 2008 Elsevier B.V. All rights reserved.
doi:10.1016/j.epsl.2008.02.025

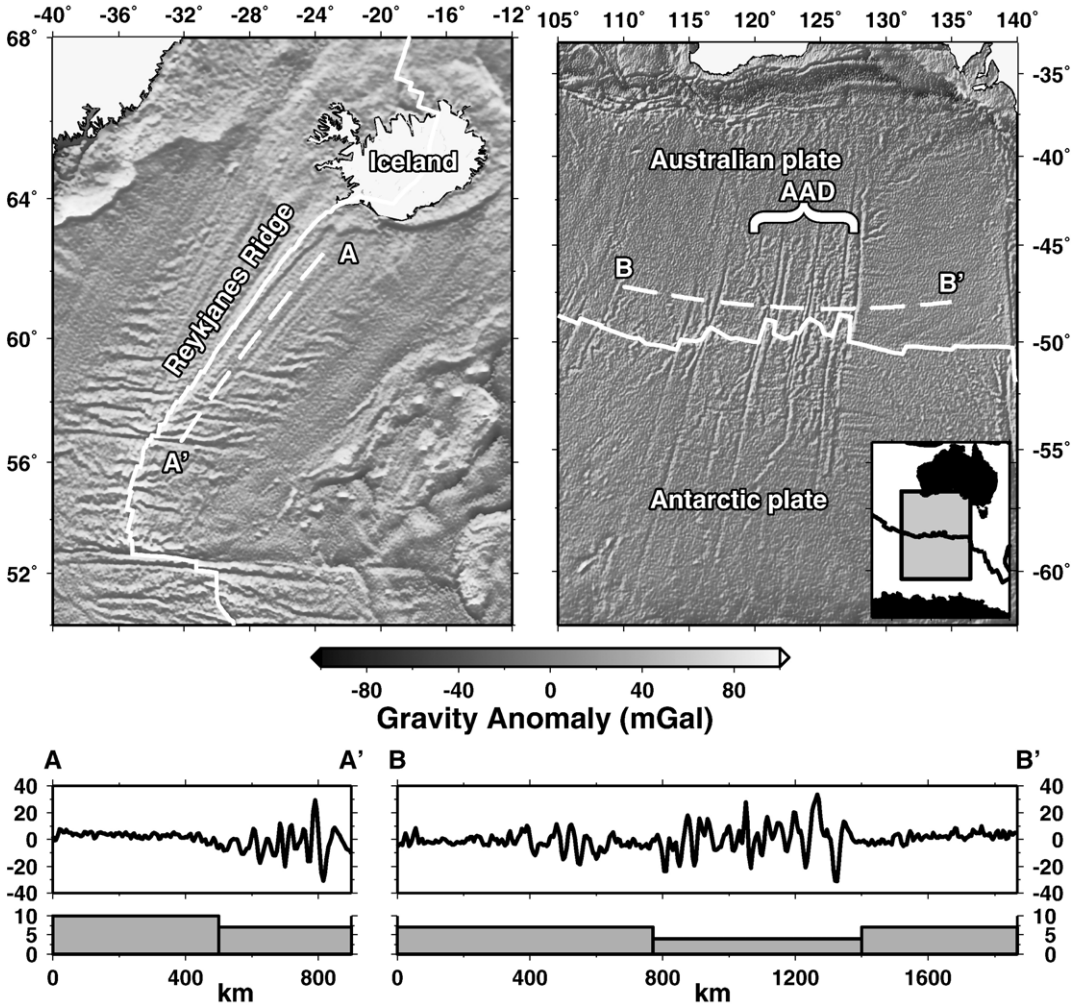

Fig. 1. Gravity anomaly maps derived from satellite altimetry of the Reykjanes ridge and the Australian-Antarctic Discordance (Sandwell and Smith, 1997). Thick white lines track the plate boundary (Bird, 2003). Each map is illuminated from the azimuths of 0° and 300°, respectively, so that the ridge-normal structures look prominent. Free-air gravity (in mGal) with mean removed (bottom panels) show the profiles (A–A' and B–B') with simplified variation of crustal thickness in km (lower plots). See text for crustal thickness references.

According to this model, the variable amount of available magma at spreading centers and its along-ridge transport are responsible for along-ridge variations in axial bathymetry and associated geophysical and geochemical observations (MacDonald et al., 1991; MacDonald, 1998). Relating mantle dynamics to the conceptual magma supply model, calculations of mantle flow beneath slow spreading centers exhibit 3-D patterns that are segmented along the axis (Parmentier and Phipps Morgan, 1990; Lin and Phipps Morgan, 1992; Barnouin-Jha et al., 1997; Madge and Sparks, 1997). A problem with such flow models is that the wavelengths of the segmented mantle upwelling are larger (150 km) than the observed average second order segment length (~50 km) (Barnouin-Jha et al., 1997). However, when the effect of melt extraction on the viscosity of the magma residual was taken into account, a much shorter wavelength of segmented flow (as short as 70 km) was achieved (Choblet and Parmentier, 2001). Related to the magma supply model, ridge migration with respect to a hot spot reference frame was suggested to cause asymmetric mantle upwelling and melt production (Carbotte et al., 2004). This model provides an explanation for the observation that the majority of "leading" segments (that is, those that step in the same direction as ridge migration direction) are magmatically more robust.

Although the magma supply model is consistent with a range of observations, the model has yet to be linked with the brittle manifestation of mid-ocean ridge segmentation. Thermal stress due to the cooling of oceanic lithosphere is one possible driving force responsible for brittle ridge segmentation among many others (cf. Kastens, 1987). Using an order of magnitude argument, Collette (1974) suggested that thermal stress associated with the cooling of oceanic lithosphere should exceed its strength. By computing the bending moment of a semi-infinite thin elastic plate experiencing top-down cooling, it was suggested that segment length should be determined such that a plate can release thermal stress by bending (Turcotte, 1974). Expanding on this theory, Sandwell (1986) showed that ridge-bounding first order discontinuities can release thermal stress effectively when their spacing is proportional to spreading rate. Decomposing thermal stress into contraction and bending components, Haxby and Parmentier (1988) speculated that thermal bending stress, not contraction, would govern the spacing of transform faults because the magnitude of thermal contraction stress was independent of the ridge segment length. These studies, however, provide only an upper bound or indirect estimate of the fracture zone spacing. Sandwell and Fialko (2004) focused on the optimal spacing between thermal cracks, which minimizes stored elastic energy in a bending plate. It is notable that the spacing is not given *a priori* but is determined by the principle of minimum elastic energy.

A theory of thermal cracks provides useful insight into the spacing of ridge discontinuities if we assume that ridge segmentation occurs due to thermal stress. The stress distribution as a function of distance from a two-dimensional crack has been analyzed by Lachenbruch (1962). In a thermally contracting elastic half space, stresses are assumed to be released on the wall of a vertical crack. At greater

distances from the wall, stress will increase to an ambient level so that each crack has a finite zone of stress relief. Since the strength of the material is limited, another crack will form at a distance where the stress exceeds the strength. In this fashion, the spacing between cracks is related to material strength and the size of the stress relief zones, which is determined by the material's elastic properties. Although this model could successfully explain crack spacing in permafrost, it leads to an apparent paradox for mid-ocean ridge segmentation. The model predicts a shorter spacing of cracks when the ambient level of stress is higher or the depth extent of cracks is shallower (Lachenbruch, 1962). Consequently, for fast and hot spreading centers, the Lachenbruch model implies a smaller fracture zone spacing because the amount of thermal stress is larger and brittle layers thinner compared to slow cooler spreading centers. In fact, the opposite trend is observed.

In this study, we investigate the role of thermal stress on the formation of mid-ocean ridge segmentation in terms of brittle deformation in young oceanic lithosphere. We address the influence of crustal thickness and rheology, factors that reflect a ridge system's tectonic setting, on fracture zone formation. A numerical method is used in which brittle deformation is allowed within the framework of continuum mechanics. This is an exploratory attempt towards a better understanding of ridge segmentation processes: relatively simple numerical models are used to draw implications relevant to actual ridge systems.

2. Numerical method

We use SNAC, an explicit finite difference code, to solve for the equations of momentum and heat energy conservation (Choi et al., in preparation). Although the code is fully three-dimensional, because of computational requirements, we only solve for 2-D problems here. The conservation equations are solved by the energy-based finite difference method (Bathe, 1996), which makes SNAC equivalent to a finite element code with linear tetrahedral elements except for the lack of explicit references to shape functions. The well-known over-stiffness of linear tetrahedral elements in the incompressible limit is overcome using a mixed discretization technique (Marti and Cundall, 1982; de Sousza Neto et al., 2005). The solution scheme is identical to that used in FLAC (Fast Lagrangian Analysis of Continua) (Cundall, 1989; Poliakov et al., 1993; Poliakov et al., 1994; Poliakov et al., 1996), where a dynamic problem is damped to achieve an equilibrium solution. An explicit forward Euler method is used for the solution integration and time-dependent constitutive update. SNAC benefits from modern software engineering through StGermain, an infrastructure framework for developing modeling software (Quenette et al., 2005).

2.1. Constitutive model for brittle and plastic deformation

Strain-weakening plasticity is coupled with viscoelasticity in our elasto-visco-plastic (EVP) model. An additive decomposition of total strain is assumed such that the total strain is the sum of elastic, viscous, and plastic strain (e.g., Albert et al., 2000). The stress update algorithm is very close to a standard rate-independent plasticity (Simo and Hughes, 2004), but the elastic trial stress is replaced with the Maxwell viscoelastic trial stress. This constitutive model enables failure mechanism, either brittle failure or viscous creep, to be selected uniquely and naturally. For example, an extremely high viscosity at low temperature would allow only a negligible amount of creep, so that material will undergo brittle failure when stressed beyond its strength. On the other hand, elastic stress would be substantially relaxed by creep if viscosity is lowered at high temperature, prohibiting brittle failure. One simplification is the use of effective viscosities derived from power laws for dislocation creep. Instead of using power laws directly for constitutive updates, the derived effective viscosities are inserted into the Maxwell viscoelastic constitutive law. We assume that stress increments at each time step are sufficiently small so that there is no need to iterate the constitutive update step when dealing with the nonlinearity of power law creeps. The term "plastic flow" often means distributed flow by creep (Rutter, 1986; Kohlstedt et al., 1995; Hirth, 2002). However, it should be distinguished from the phenomenological plasticity for brittle deformation used in this study. It is the viscous component in our EVP constitutive model that corresponds to such non-localized flow.

Brittle deformation is characterized by the rapid loss of cohesion after yielding (Jaeger and Cook, 1976) and becomes localized into narrow fault zones. Assuming a strain-weakening rule, a classical plastic constitutive model can lead to brittle failure. Localization is meant to be an outcome of the bifurcation inherent to strain-weakening plasticity (Rudnicki and Rice, 1975) rather than of special boundary conditions or the geometry of the domain. The Mohr–Coulomb criteria for fracture strength is adopted and specified by an internal friction angle (φ), a dilation angle (ψ), and cohesion (c). Cohesion is only poorly constrained by experiments, but we take rough estimations based on previous publications: 44 MPa for oceanic crust (Lavier et al., 2000) and 150 MPa for dunite (Hirth, 2002). The weakening rules define cohesion as piecewise linear functions of a non-negative scalar representing the amount of accumulated plastic strain, $(\lambda'^2_1+\lambda'^2_2+\lambda'^2_3+\theta^2)^{1/2}$, where λ'_i is the i-th principal value of deviatoric plastic strain and θ is the volumetric plastic strain (Lavier et al., 2000; Lavier and Buck, 2002). For simplicity, we fix plastic parameters as well as the weakening rule for all models in this paper (Table 2).

2.2. Thermo-mechanical coupling

SNAC computes a time dependent temperature field by solving the equation of heat energy conservation. The resultant temperature variations are coupled to pressure change through thermal expansion coefficient and bulk modulus (Boley and Weiner, 1960). Although an energy feedback through work done by volume change and shear heating (e.g., Regenauer-Lieb and Yuen, 2004; Kaus and Podladchkov, 2006) are potentially significant, we do not consider them. This simplification is justified by the fact that brittle failure in the form of thermal cracks is essentially tensional although gravity always adds small shear components. The transient nature of thermal stress also supports this one-way coupling. Unlike problems driven by persistent boundary loading, here thermal stress is the only driving force. Once thermal stresses are released by brittle failure, energy dissipation in the failed regions cannot be sustained.

3. Model setup

A series of 2-D models are constructed to represent a vertical cross-section along a straight ridge segment (Fig. 2). A 500 km long and 50 km deep domain is discretized into 1×1 km quadrilateral elements. To avoid complexities involving ridge axial processes, the domain is assumed to be initially at a small distance from the spreading center such that the initial temperature field is 0.3 My old lithosphere given by a half-space cooling model. Temperature is fixed at 0 °C on the top surface and 1350 °C at the bottom. The effect of hydrothermal cooling is taken into account (e.g., Chen and Morgan, 1990b) through a time-dependent thermal conductivity of crust that is defined as $k=k_0+k_1\exp(-t/\tau)$, where k_0 is the normal value for crust's thermal conductivity, k_1 is the increment for the enhanced cooling, t is time, and τ is the decay time (fixed at 1 My). This represents the decay of the intensity of hydrothermal circulation with distance from a spreading center (Anderson et al., 1977). The initially high value of k is not a necessary condition for the occurrence of brittle deformation, but is assumed because of the important role that hydrothermal activity plays in transporting heat within young oceanic crust (Chen and Morgan, 1990b). Horizontal heat fluxes are assumed to be zero on the

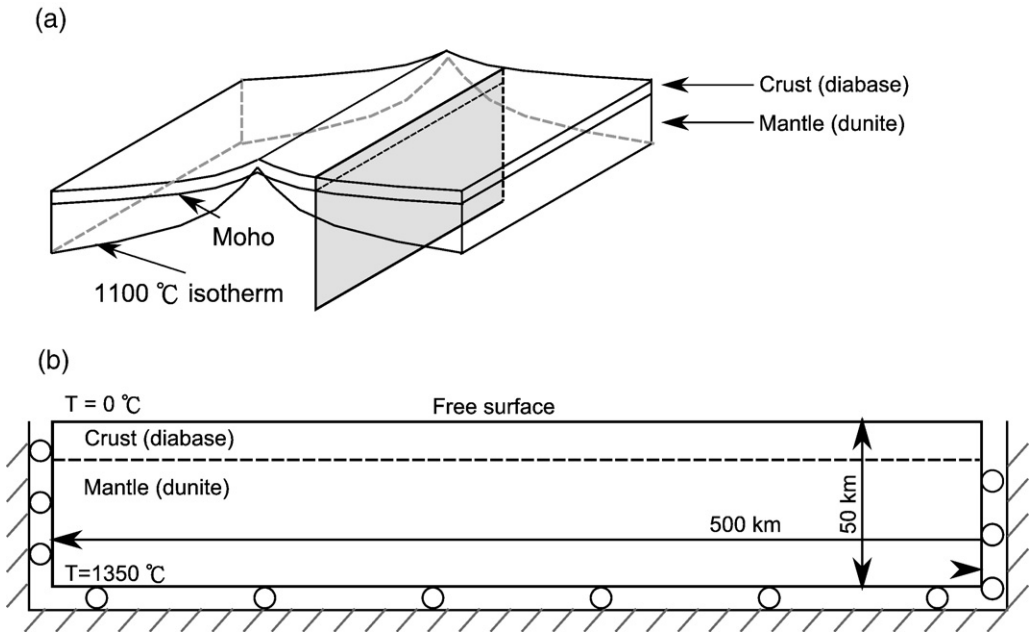

Fig. 2. Model geometry and boundary conditions. (a) The model domain is a vertical 2-D plane parallel to the ridge axis. The hypothetical ridge segment is assumed to be straight. The oceanic lithosphere has two layers. Temperature change by cooling within the domain is equivalent to tracking a newly formed slice of lithosphere (shaded plane) with time. (b) The domain is 500 km and 50 km deep. Crust and mantle are assumed to be composed of diabase and dunite, respectively. Kinematic boundary conditions are free-slip for all the surfaces except the top one, which can deform freely. Temperature is fixed at 0 °C on top and at 1350 °C on the bottom. The initial temperature field is given by the analytic solution for half-space cooling model with the age of 0.3 My.

side walls. The side and bottom boundaries have free-slip boundary conditions while the top boundary is a free surface. All the models were integrated for 10 My.

For power law creep rheologies, we use two different sets of data that represent weak and strong lower crusts, respectively. The material parameters for weak lower crust are taken from the experimental data compiled by Kirby (1983). The corresponding mantle rheology is that used by Chen and Morgan (1990b) and Shaw and Lin (1996). This weak crustal rheology has been questioned because crustal rocks cannot be as wet as the specimens used in those experiments (e.g., Hirth et al., 1998). So, for comparison, rheologies for strong lower crust composed of dry diabase (Mackwell et al., 1998) and dunite (Chopra and Patterson, 1984) are also used.

Crustal thickness is varied so as to represent several different tectonic environments. Crustal thickness and its along-axis variations are sensitive to plate tectonic environments. For instance, fast spreading centers have relatively uniform thicknesses whereas slow ones show Moho depth variations of a few km (MacDonald et al., 1991; MacDonald, 1998). In addition, proximity to hot spots or cold mantle is also known to affect crustal thickness (e.g., Smallwood and White, 1998). Crustal thickness was emphasized in the context of the axial

Table 1
List of numerical experiments

Model	Crustal thickness	Type of rheology	Plastic flow
1	Normal (7 km)	Weak*	Associated
2	Thin (4 km)	Weak	Associated
3	Thick (10 km)	Weak	Associated
4	Normal	Strong**	Associated
5	Thin	Strong	Associated
6	Thick	Strong	Associated
7	Normal	Weak	Non-associated
8	Thin	Weak	Non-associated
9	Thick	Weak	Non-associated
10	Normal	Strong	Non-associated
11	Thin	Strong	Non-associated
12	Thick	Strong	Non-associated
13	The same with model 1 except T_{mantle} = 1250 °C		
14	The same with model 2 except T_{mantle} = 1250 °C		
15	The same with model 4 except T_{mantle} = 1250 °C		
16	The same with model 5 except T_{mantle} = 1250 °C		

* Chen and Morgan (1990a).
** Mackwell et al. [34] for crust and Chopra and Paterson [14] for mantle.

Table 2
Rheological model parameters

Symbol	Description	Model value
ρ_c	Density of crust	2900 kg/m^3
ρ_m	Density of mantle	3300 kg/m^3
λ	Lame's constant	Crust: 30 GPa Mantle: 60 GPa
μ	Shear modulus	Crust: 30 GPa Mantle: 60 GPa
A	Pre-exponential coefficient	Crust: 100 (100)* Mantle: 1000 (28840)*
H	Activation enthalpy	Crust: 260 (485)* kJ/mol Mantle: 520 (535)* kJ/mol
n	Stress exponent	Crust: 3.4 (4.7)* Mantle: 3.0 (3.6)*
$\dot{\varepsilon}_{ref}$	Reference strain rate	10^{-16} s^{-1}
k_0	Enhanced thermal conductivity	7.5 Wm^{-1} K^{-1}
k_1	Normal thermal conductivity	3.0 Wm^{-1} K^{-1}
τ	Decay time for thermal conductivity	1 My
c_p	Isobaric heat capacity	1100 J kg^{-1} K^{-1}
α_v	Volumetric thermal expansion coefficient	3.2×10^{-5} K^{-1}
R	Gas constant	8.3145 Jmol^{-1} K^{-1}
φ	Friction angle	30°
Ψ	Dilation angle	30° or 0°
C_0	Initial cohesion	Crust: 44 MPa Mantle: 150 MPa
$\varepsilon_{ps,1}$	Parameters for piecewise linear strain softening	0.01
C_1		0.22 MPa
$\varepsilon_{ps,2}$		0.05
C_2		4.4 kPa
$\varepsilon_{ps,3}$		1000
C_3		0 kPa

* Values for the weak rheology; values within the parentheses for the strong rheology.

morphology of spreading ridges due to the potential "decoupling" effect (Chen and Morgan, 1990a). If crust is sufficiently thick, then it can have a weak lower crust that decouples the brittle upper part from the mantle. The wide decoupling zone leads to plastic failure concentrated only at the spreading center and topography close to isostatic equilibrium. In contrast, a narrow decoupling zone enhances the degree of coupling between crustal deformation and mantle flow such that necking occurs in a finite plastic failure zone creating an axial valley (Chen and Morgan, 1990a). Chen and Morgan (1990a) used this model to explain the presence or absence of an axial valley at spreading centers that have anomalously thin or thick crust for their spreading rate. The causes for anomalous crustal thickness could include proximity to a hot spot, anomalous mantle temperature, or the cold edge effect at the ridge-transform intersection. Bell and Buck (1992) also suggested that thick crust due to hot spot activity might compensate for the influence of 3-D upwelling, implying that tectonic environments can differentiate the patterns of ridge segmentation even without variations in mantle flow. To investigate this potentially critical role of crustal thickness, models have one of the following three values: Thin (4 km), normal (7 km), and thick (10 km). For simplicity, models do not include lateral variations of thickness. The complete list of models and parameter values is given in Table 1 and 2, respectively.

4. Results

4.1. Models with weak crust

The temporal evolution of topography, temperature, viscosity, and plastic strain for the model with weak and normal thickness (7 km) crust (model 1 in Table 1) is shown in Fig. 3. The viscosity field is almost entirely determined by temperature while the dependence on stress is minimal. Lower viscosities are consistently found in the lower crust. Although brittle deformation occurred in the high viscosity uppermost part of the crust and mantle, the amount of plastic strain was only about 1%. The initially uniform brittle deformation in the mantle started to evolve into regularly spaced discrete zones at 4 My. These discrete brittle zones have a visually estimated spacing of 7–10 km. Cooling continues to drive brittle deformation so that by 7 My, some discrete brittle zones have started to accumulate more strain at the expense of others. We term the further growing brittle zones "primary cracks" and those that stopped growing "secondary cracks". These terms are defined in a relative sense at any given time. Some primary cracks at one time might become secondary later if only a selected subset of the primary cracks continue to grow. Fig. 4 shows magnified images of the upper-left part of the domain in Fig. 3. The images compare the plastic strain and the second invariant of deviatoric stress

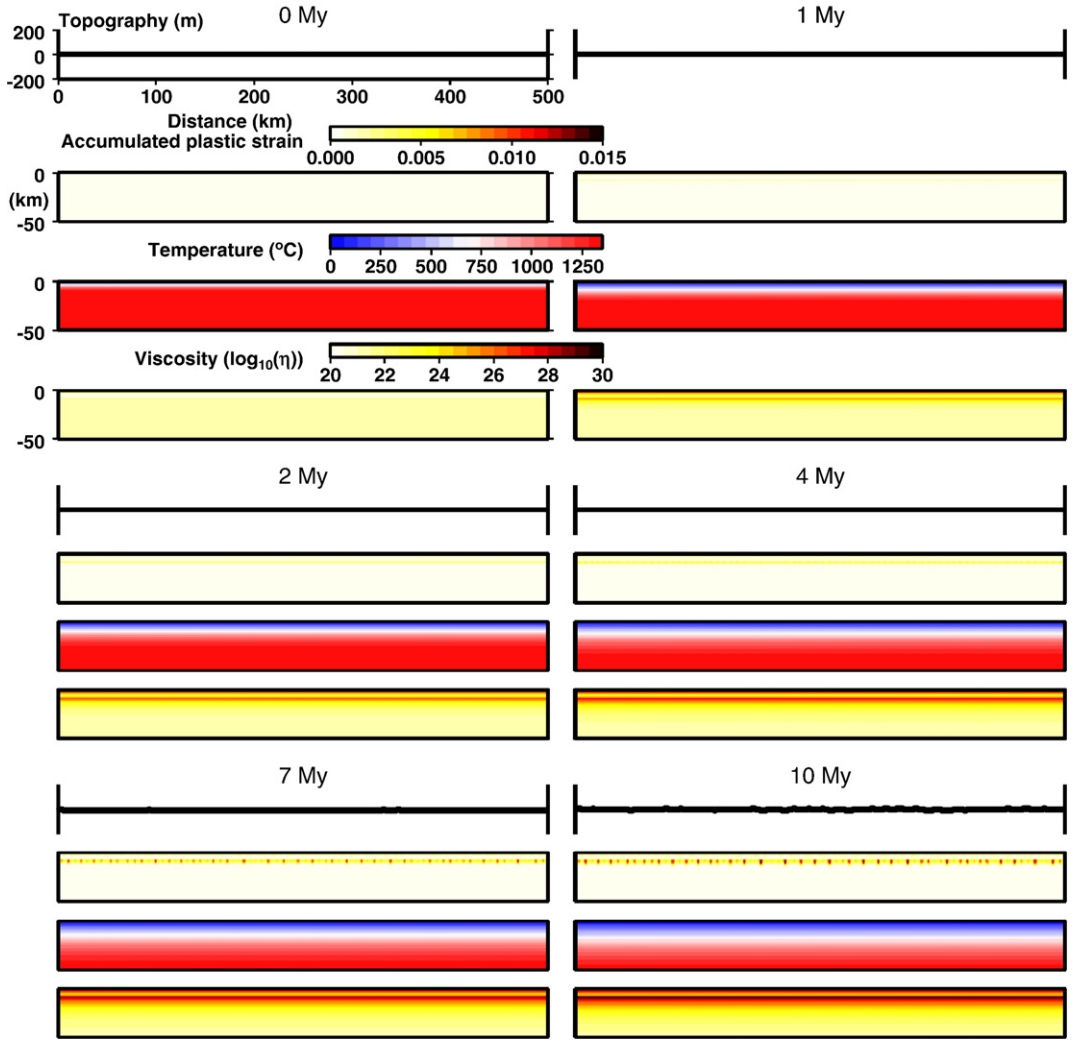

Fig. 3. Evolution of topography, temperature, viscosity, and brittle deformation (plastic strain) for the model with weak and normal thickness crust (model 1). Viscosity fields directly reflect temperature change, but low-viscosity lower crust highlights the two-layer structure. Brittle zones (with a ~10 km spacing) start to emerge by 7 My, and some brittle zones continue deforming as cooling proceeds. These later brittle zones create valleys on surface with a relief of about 20 m by 10 My.

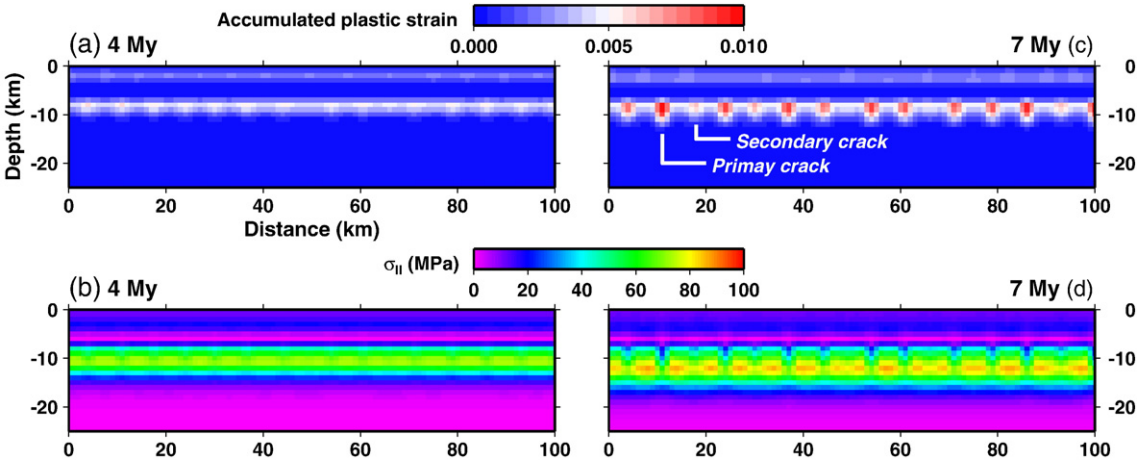

Fig. 4. The upper left part of the model shown in Fig. 3 is magnified to compare the brittle zones at 4 and 7 My. Each panel covers 0–100 km in the ridge-parallel direction and 0–25 km in depth. The accumulated plastic strain and the second invariant of deviatoric stress (σ_{II}) at 4 My are shown in (a) and (b), respectively; those at 7 My in (c) and (d).

(σ_{II}) at 4 and 7 My and show the selective growth of primary cracks from a set of initial cracks that are more numerous and finely spaced. The maximum of σ_{II} increases with the depth extent of brittle zones because it is constrained by a linear pressure-dependence of the yield stress, like strength envelopes used in previous studies (e.g., Parmentier and Haxby, 1986; Haxby and Parmentier, 1988; Wessel, 1992). As seen from the plastic strain (Fig. 3), the primary localized zones of brittle deformation that continue to grow after 7 My have a spacing of about 15–25 km. The overall subsidence of topography occurs because of isotropic thermal contraction. So, the topography at a given time step is presented with the mean removed. No cracks could completely penetrate the whole crustal layer. Even the primary cracks did not create significant topographic relief on the top surface. Nucleated in the uppermost mantle, they did not propagate into the overlying lower crust. This discontinuity of brittle deformation across the lower crust is consistent with the existence of a weak lower crust.

Models with different crustal thicknesses follow the same sequence of brittle deformation: Initially uniform brittle deformation in the high viscosity regions, subsequent localization forming discrete brittle zones, and differentiation of brittle zones into primary and secondary cracks. However, they also produced significant differences in terms of the distribution of plastic strain and topography (Fig. 5a). We summarize results from two models for a weak crust (model 2 and 3 in Table 1), of which crustal thickness is varied from 7 km (normal) to 4 km (thin) and 10 km (thick), respectively. They are compared to the normal thickness model described above.

The thin crust model created grabens and half-grabens with ~50 m of subsidence and a 100–150 km spacing (Fig. 5a). The topography between grabens is concave upward, indicating that thermal contraction is stronger in the upper part than in the lower part of lithosphere so that a positive bending moment is generated. In contrast to the normal crustal thickness model, the model with the thin crust accumulated more plastic strain (maximum ~4%). The primary brittle zones connected to grabens clearly show a V-shaped distribution of accumulated plastic strain that is continuous across the lower crust. These differences between the normal (7 km) and thin (4 km) crust

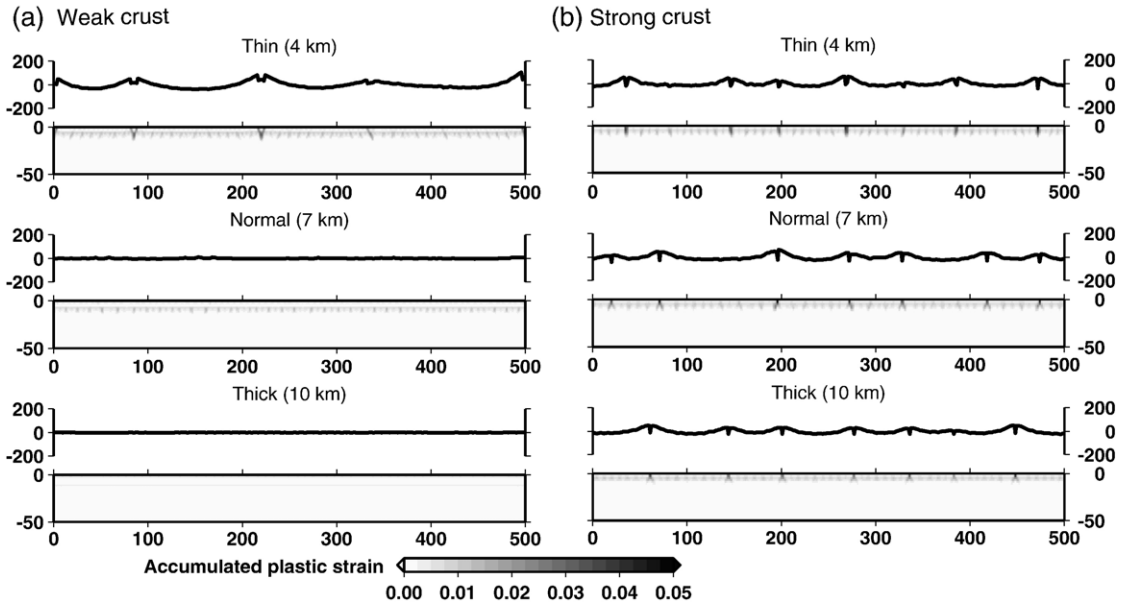

Fig. 5. Topography (in m) and accumulated plastic strain for the models with associated plasticity at 10 My. (a) Weak crust models with varied crustal thicknesses (model 1–3 in Table 1). (b) Models with the strong crustal rheology (model 4–6).

models can be attributed to differences in temperature within the lower crust. In the thin crust model, lower crust is colder and the exponential dependence of viscosity on temperature renders the lower crust essentially brittle.

The thick crust model accumulated a plastic strain of only ~0.4%, negligible compared to the values from models with thinner crust, and the topography is essentially flat (Fig. 5a). Although the highly viscous parts of the model did yield, the deformation never localized. Thus, the thick crust model did not develop topography associated with primary cracks other than the uniform subsidence due to thermal contraction.

4.2. Models with strong crust

The model with a strong and 7 km-thick (normal thickness) crust (model 4 in Table 1) is clearly distinguished from those of the weak crust models in terms of plastic strain and viscosity (Fig. 6). The two-layer structure of crust is obscured in this model's viscosity because lower crustal viscosities are consistently higher. Persistently active primary cracks are vertical and emerge as early as at 1 My with a spacing of 70–100 km. The topography is characterized by narrow troughs connected to primary cracks and the concave upward segments between the troughs. In contrast to the weak crust models, the primary cracks are nearly vertical, not V-shaped, and develop much earlier: it required 4 My in weak models (Fig. 3), 1 My in this case.

Reduced or increased crustal thickness in the strong crust models (model 5 and 6 in Table 1) did not have as strong an influence as in the weak crust models (Fig. 5b). All the models are similar in terms of temporal evolution and resultant topography although the position of primary cracks was not fixed in space. Amplitude of the concave upward topography in the trough-bounded segments is nearly constant regardless of crustal thickness.

Models with different crustal thicknesses show differences in the geometry and propagation depth of primary cracks (Fig. 5b). The models of normal and thick crust have primary cracks that are vertical near the surface and branch towards greater depths, making an inverted V-shape. In contrast, the primary cracks in the thin crustal model remain vertical throughout their vertical extension. The propagation depth is about 10 km in the models with thin and normal crust, while it is smallest with a thick crust (~5 km). The maximum of accumulated plastic strain is similar in all three strong crust models, but the secondary cracks of the thin crust model exhibit larger plastic strain than the other models.

4.3. Non-associated plasticity

The previously described results were obtained under the assumption of an associated flow rule: i.e., the dilation angle was set to be equal to the friction angle. We took advantage of the associated flow rule as a numerical means to achieve significant opening in the band of localized strain. However, non-associated flow rules, in which

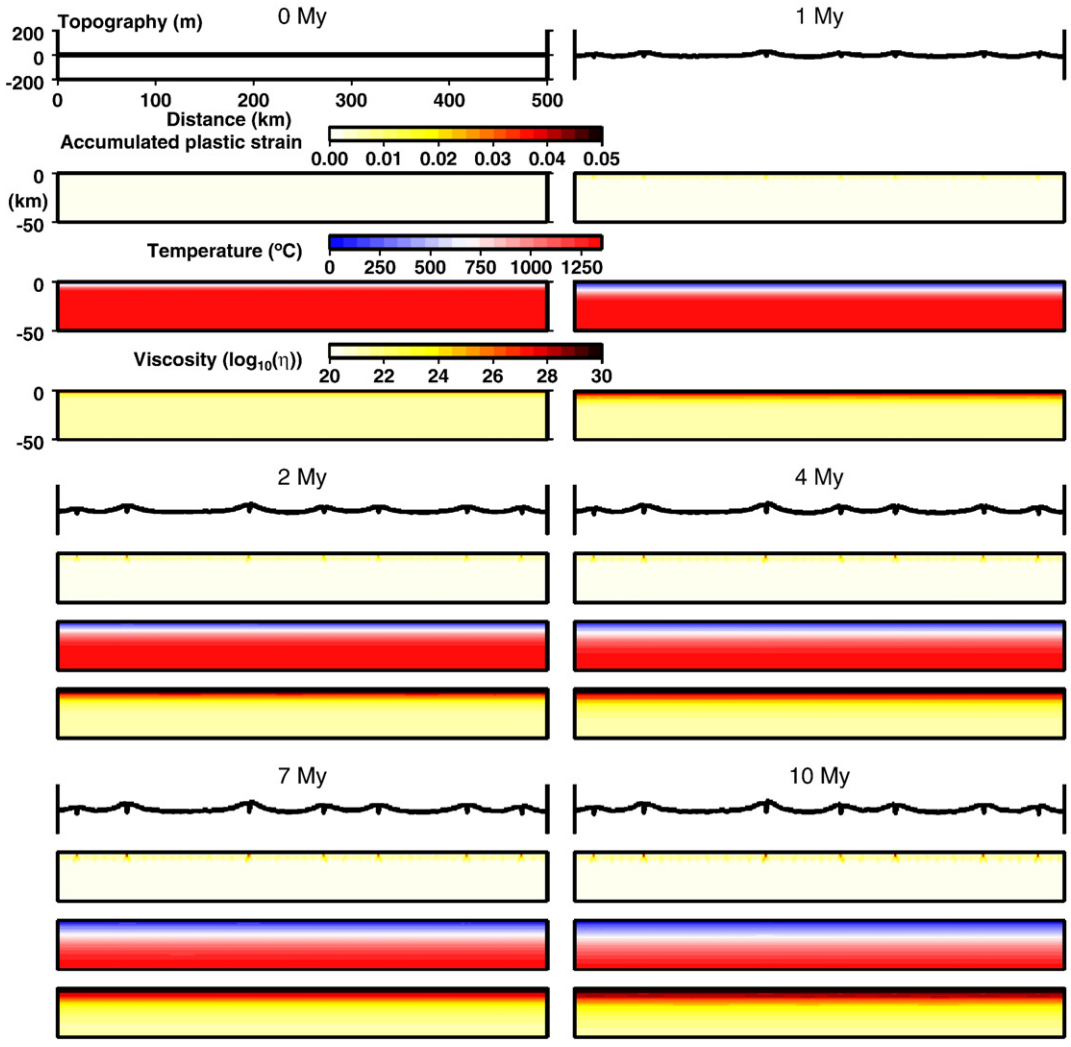

Fig. 6. Same as Fig. 3, but the results from the model with a strong and 7 km-thick (normal thickness) crust.

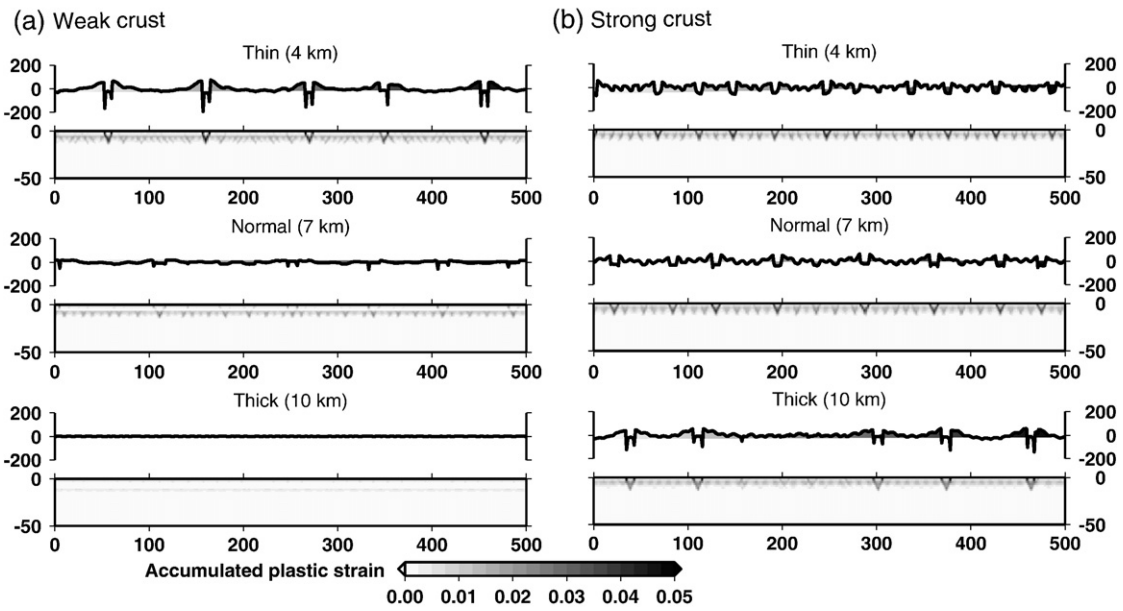

Fig. 7. Same as Fig. 5, but for the models with zero dilation angle. (a) Weak crust models with varied crustal thicknesses (model 7–9 in Table 1). (b) Models with the strong crustal rheology (model 10–12).

dilation angle is not equal to the friction angle, are usually considered more appropriate for frictional materials like rocks (e.g., Rudnicki and Rice, 1975). Among the possible choices of non-associated plasticity, the assumption of plastic incompressibility, i.e., with a dilation angle of 0° was suggested in studies of shear bands in rocks (e.g., Poliakov and Hermann, 1994). Although this condition is extreme in the sense that volumetric plastic strain is completely prohibited, we evaluate its effects for comparison. Models with strong and weak crustal rheology as well as variable crustal thickness were computed with a dilation angle of 0° (model 7–12 in Table 1). Since all the other parameters and the initial and boundary conditions were the same as described in the previous two sections, these models followed a very similar sequence of temporal evolution while exhibiting substantial differences at the same time. The assumption of plastic incompressibility enables only shear bands to appear, not cracks with opening. However, we use the descriptive terms, primary and secondary cracks, for continuity with the previous discussion. In the following, regardless of the rule used for plastic flow, a primary crack refers to a localized band of plastic strain that penetrates crust and creates a topographic signature, while localized plastic strain that stopped growing before propagating into crust are called secondary cracks.

Differences found in the weak crustal models involve the geometry of primary cracks and resultant topography (Fig. 7a). Among the models with a weak crust, only the one with thin crust developed significant topography. As in the models with an associated flow rule, this model shows V-shaped primary cracks, which create grabens on the top surface spacing and relief larger than those cases with the associated flow rule (Fig. 5a). The maximum plastic strain, ~5%, is larger than 1.5% of the corresponding model of an associated flow rule. The spacing of primary cracks decreased slightly compared to the counterpart with an associated flow rule such that it shows a range of 80–110 km.

The non-associated plasticity in the strong crustal models also resulted in differences in the brittle deformations (Fig. 7b). In contrast to the corresponding models with non-zero dilation angle (Fig. 5b), all the strong crustal models developed V-shaped primary cracks and associated grabens. The spacing of primary cracks shows a clear positive correlation with the thickness of crust. The average spacing of primary cracks varies from 49 km in the thin crust model to 99 km in the thick crust model (Table 3). When the associated flow rule was used, the relationship between the spacing of primary cracks and crustal thickness was not clear (Fig. 8a).

5. Discussion

5.1. Effects of crustal thickness and creep strength

The models show that creep strength and crustal thickness strongly influence brittle deformation by the release of thermal stresses. Through the centers of surface troughs (grabens) that are connected to the primary cracks at depth, we measure the average spacing between the primary cracks (Table 3; Fig. 8).

Crustal thickness determines whether primary cracks are created. If the crust is thicker than a global mean (6–7 km, Chen, 1992; White et al., 1992) and thus has a weak lower part, then the primary cracks do not develop as the stress in the uppermost mantle is released through creep before being transferred to the surface. When the crust is thinner than a threshold value, the entire crustal layer becomes sufficiently cold and strong to create primary cracks. If the creep strength of the crust is “strong”, then the role of crustal thickness is less important than when the crust is weak. When the lower crust is sufficiently strong, then primary cracks are always created, at least for the range of crustal thicknesses tested.

When the non-associated flow rule is used in the models, crustal thickness clearly determines the spacing of primary cracks. When a non-associated flow rule is assumed by setting the dilation angle to zero, plastic strain cannot have a volumetric component. Models with

Table 3
Summary of average spacing of primary cracks at 10 My

		Associated	Non-associated
Strong	Thin	73±23 km*	47±13 km
	Normal	76±28 km	62±17 km
	Thick	71±22 km	105±50 km
Weak	Thin	125±34 km	100±14 km
	Normal	N/A	N/A
	Thick	N/A	N/A

* Mean±standard deviation.

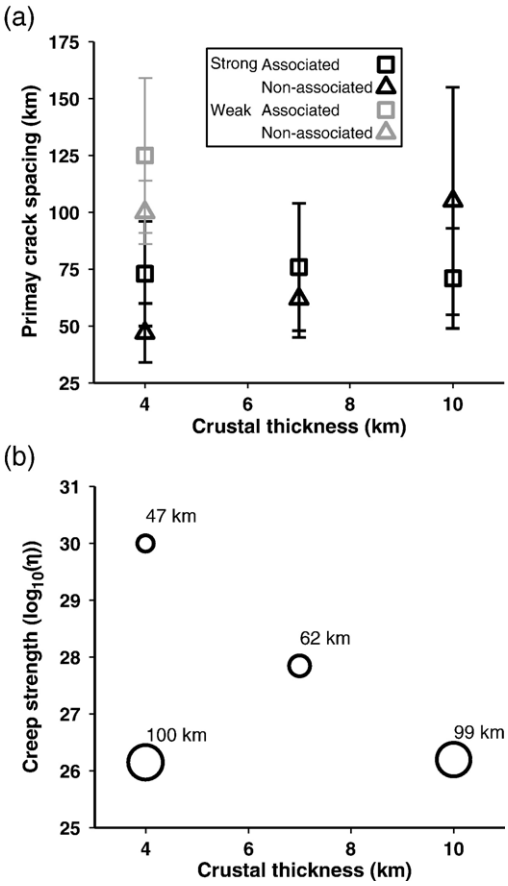

Fig. 8. (a) Plot of the primary crack spacing at 10 My versus crustal thickness for different combinations of crustal rheology and the plastic flow rule. (b) Plot of the primary crack spacing with respect to crustal thickness and creep strength of lower crust. Only the cases with non-associated plasticity are plotted. The crack spacing is denoted by labels and also represented by the sizes of symbols. The creep strength is represented by the logarithm of viscosity ($\log_{10}(\eta)$) taken from the bottom layer of crust in each model at 10 My and the values of the other parameters are listed in Table 3.

a zero dilation angle demonstrate this effect by creating primary and secondary cracks in the non-vertical maximum shear direction determined by thermal stress and gravity. In addition, when the crust is strong, the spacing between primary cracks is proportional to crustal thickness: as the crustal thickness increases from 4 to 10 km, spacing increased from 49 to 99 km (see the trend of black triangles in Fig. 8a). This relationship can be placed within the context of Lachenbruch's analysis (1962). The temperature drop at 4–7 km depth leads to thermal stresses in either the crust or mantle that depends on crustal thickness. Since the mantle's elastic moduli are larger than those of the crust, the amount of thermal stress is larger when the crust is thin, while smaller thermal stresses are available in the thick crust model. According to the theory of thermal cracks, when the ambient stress (i.e. thermal stress prior to brittle deformation) is higher, the spacing of thermal cracks decreases because the size of stress relief zone shrinks. As a result, the thinner crust develops more finely spaced primary cracks.

One of the parameters Lachenbruch (1962) considered important in determining the crack spacing is the depth extent of cracks. In his analysis, the deeper cracks have a larger zone of stress relief resulting in a larger crack spacing. However, in our models, cracks always stop propagating downward at some depth regardless of their class, primary or secondary, because yield stress increases with pressure. In spite of more or less constant depth extent of primary cracks, the differences in the crack spacing are still observed, indicating that the vertical extent is not a major controlling factor determining crack spacing compared to crustal thickness and creep strength.

Another contribution to the correlation between crustal thickness and crack spacing comes from elastic unloading that occurs outside a shear band after the onset of localization (Vermeer, 1990). Elastic unloading occurs only when the plasticity is non-associated, and the amount of unloading is proportional to yield stress (Vermeer, 1990; Le Pourhiet, *pers. comm.*) Being pressure-dependent, the yield stress of mantle directly below the Moho is smaller when the crust is thin compared to when it is thick. Consequently, a thin crust experiences a small stress drop with a relatively large ambient stress as a result, while a thick crust goes through a large stress drop reaching a relatively small ambient stress. The different values of ambient stress due to different crustal thickness leads to variations in the primary crack spacing as inferred from Lachenbruch's model described above. Furthermore, the lack of elastic unloading might be the reason the correlation is not obvious in the models with associated plasticity.

5.2. Implications of the sensitivity to crustal thickness and creep strength

The sensitivity of the spacing of primary cracks to crustal thickness suggests that the non-uniform tectonic environment of a mid-ocean ridge system can exert a fundamental, but indirect, control over local changes in the ridge system's brittle deformation. Non-uniform mantle temperature and proximity to hot spots can indirectly contribute to brittle deformation through spatial and temporal variations in crustal thickness. For instance, models with mantle temperatures that are low (models 13–16 in Table 1) demonstrate the relative insignificance of mantle temperature (Fig. 9). With the mantle temperature of 1250 °C, lower than in models 1–12 by 100 °C, the magnitude of thermal stress still exceeds the brittle strength of oceanic lithosphere by a substantial amount at shallow depths. As a result, the relationship between crustal thickness and primary cracks is the same as in those models with a higher mantle temperature. Similarly, the effects of creep strength are not much modified by lowered mantle temperature: The stronger crust has a higher threshold thickness, below which topography associated with primary crack can be created as in the models with a higher temperature. Consequently, a 7 km-thick crust can develop primary cracks when the lower crust is strong (Fig. 9).

Evidence for the causal relationship between crustal thickness and the brittle deformation of oceanic lithosphere can be found along the Reykjanes ridge and the Australian-Antarctic Discordance (Fig. 1). The crust of the Reykjanes ridge is known to be thicker than 10 km (e.g., Smallwood and White, 1998). The lack of fracture zones in this ridge system appears consistent with the subdued brittle deformation and the lack of primary cracks in the thick crust models. The distinction between the Reykjanes ridge and other slow-spreading centers has previously been attributed to thick crust (Chen and Morgan, 1990b; Bell and Buck, 1992). The opposite effects of a thin crust are found in the AAD. The evolution of the AAD was reconstructed by Marks et al. (Marks et al., 1999). They suggested that the increase in the number of ridge segments and their offset might be a local outcome of amagmatic extension rather than of regional influence from cold mantle. Based on the detailed observations on the central region of the AAD, Okino et al. (2004) identified asymmetric spreading on oceanic detachments as a dominant mode of extension and attributed it to low magma supply and cold mantle. Our models with the lowered mantle temperature suggest that the reduced amount of thermal stress due to the cooler mantle is not as significant for brittle deformation as the reduced crustal thickness. We can infer that the magma-starved spreading centers produce thinner crust, and the thinner crust, as shown in this study, facilitates brittle deformation due to cooling, resulting in more rugged topography and more fracture zones.

In addition to crustal thickness, our results also show a strong sensitivity of brittle deformation to creep strength of the crust and mantle. Our models show that primary cracks are created regardless of crustal thickness when a high creep strength for dry diabase is used, while crustal thickness governs the degree of fracturing when creep

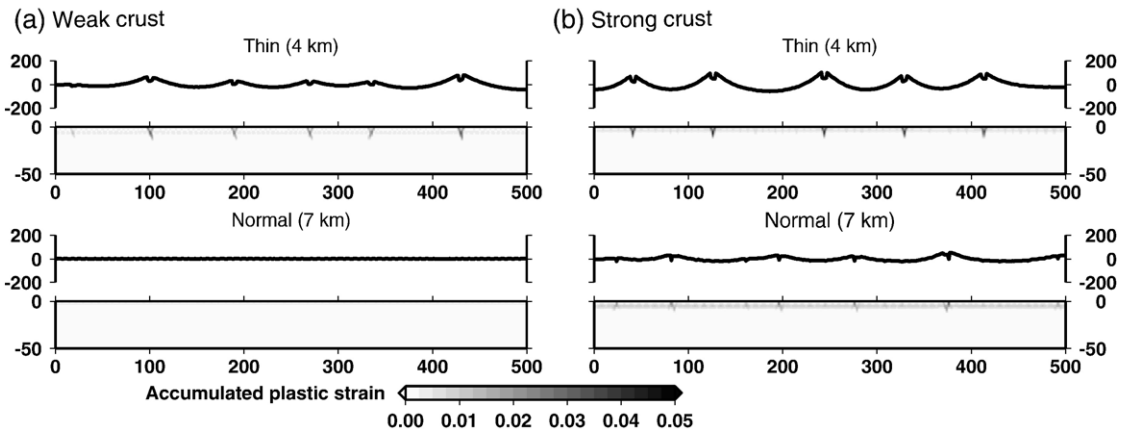

Fig. 9. Same as Fig. 5, but the mantle temperature is lowered to 1250 °C from 1350 °C.

strength is low. However, experiments and observations suggest that the mid-ocean ridge basalts and gabbros are only 5% saturated with water (Hirth et al., 1998). Even at the wet hot spot like the Reykjanes ridge, the observed maximum water content of 0.4 wt.% (Nichols et al., 2002) is, although relatively high, is only 10% of the solubility (e.g., Dixon et al., 1995). Therefore, the major effect of the higher water content at the Reykjanes ridge would be an enhanced degree of melting and thus a thicker crust rather than lowered creep strength. The weakening effect due to the wet mantle source, however, cannot be completely ignored. Our results showed that even the thick crust developed primary cracks when the creep strength of dry diabase was used, which is in contrast with the lack of fracture zones at the Reykjanes ridge. The surface topography was comparably smooth only in the models with weak creep strength.

The spacing of primary cracks from our models is mapped to a two-dimensional space spanned by the crustal thickness and lower crust creep strength (Fig. 8b). For non-associated plasticity, models with thin and strong crust has the smallest crack spacing and crack spacing increases as the crust becomes thick and weak (Fig. 8b). This relationship is expected because the creep strength of lower crust is determined by the crustal thickness. Another trend is found between the crack spacing and the creep strength for a constant crustal thickness (4 km), where the crack spacing is inversely proportional to the creep strength. In addition, sufficiently weak lower crusts with the creep strength of ~10^{26} Pa s do not show significant correlation with thickness. These trends suggest that creep strength and crustal thickness can independently influence crack spacing.

5.3. Flexure of the segments

The upward concavity of all the primary crack-bounded segments indicate that primary cracks impose local boundary conditions so that the segments are free to contract horizontally, which generate a compressional stress field on the top of a cooling and growing plate as shown in previous studies (Parmentier and Haxby, 1986; Haxby and Parmentier, 1988; Wessel, 1992). The free-slip boundary conditions of the whole domain prohibit horizontal contraction and might be expected to result in a stress field with the opposite sign. A cooling plate with its boundaries fixed develops tension on the top due to inhibited contraction (e.g. Turcotte, 1974). The boundary conditions of the whole domain initially do lead to the buildup of tensional stresses on the top of lithosphere, but only until cracks appear. The full thermal stresses can be decomposed into thermal contraction stresses and thermal bending stresses for convenience (Turcotte, 1974; Haxby and Parmentier, 1988). The formation of crack-bounded segments releases the thermal contraction stresses and render the boundary conditions of the whole domain irrelevant for the behavior of the segments. The segments, now with nearly free boundary conditions imposed by the weak primary cracks, subsequently deform with the remaining thermal bending stresses. Through this sequence of events, the concave upward topography of a freely-shrinking plate is obtained even though the domain itself does not horizontally contract.

5.4. Implications on the ridge axial processes

The plane strain assumption implies that the cracks would extend all the way to the spreading centers, essentially determining the lengths of ridge segments. If we assume that the primary cracks correspond to fracture zones, the spacing of transform faults and associated fracture zones can be interpreted as that of primary cracks. However, this model must be too simple to be applied to actual mid-ocean ridges. For instance, a young and hot lithosphere near fast-spreading centers would not have accumulated sufficiently large thermal stress and even the available thermal stress is efficiently released by creep rather than by brittle deformation. As a result, thermal cracks initiated off-axis might not have a dominant control on the near-axis brittle deformations including the spacing between first order discontinuities. On the other hand, the increased number of primary cracks in a thin crustal model suggests that the undulating crustal thickness at slow-spreading centers might determine the locations in such a way that brittle deformation occurs only at the relatively thin parts. It might be also possible that hydrothermal cooling is enhanced along thermally induced fractures triggering magmatic segmentation with a similar spacing. Since these hypotheses now include the second-order segments with associated crustal thickness variation and spatially cover both on- and off-axis regions, fully 3-D models as well as magma dynamics would be required to address such possibilities.

The along-axis variations of crustal thickness appear necessary for achieving the observed topographic amplitude. The relief across the primary cracks as well as within a segment is 10 s to 100 m, which is considerably smaller than that of actual fracture zones (≥1 km). A simple calculation assuming isostatic equilibrium shows that 3 km of crustal thickness difference between the center and the edge of a segment can cause a relief of about 500 m, a significant contribution on top of bending due to thermal stress (~100 m). There is also a large discrepancy between the observed length of the first order segments and the primary crack spacing of our models: The observed lengths are 600±300 km along fast spreading ridges and 400±200 km for slow ones (MacDonald et al., 1991) while the segments bounded by primary cracks in our models are consistently shorter than 200 km. The values from our models (Table 3) are closer to lengths of the second order segments: 140±90 and 50±30 km for fast- and slow-spreading ridges, respectively (MacDonald et al., 1991). The discrepancy and the similarity might be only apparent because the

association of primary cracks with fracture zones is an assumption and our models cannot have true second order segments that show crustal thickness variations and temporal changes in length. In any case, improved knowledge on the rheological properties and failure mechanism is one of the pre-requisites for a more quantitative analysis of the crack spacing from numerical models.

6. Conclusions

We show that crustal thickness, crustal creep strength, and the rule for plastic flow can substantially influence the brittle deformation of oceanic lithosphere. Crustal thickness determines whether brittle deformation would evolve into primary cracks or stay at secondary cracks without associated topographic features. Primary cracks only emerge when a crust is thinner than a certain threshold. Lower crustal creep strength has a net effect of shifting this threshold: When the creep strength is higher, the threshold is raised so that primary cracks emerge even when the crust is 10 km-thick. In contrast, a weaker crust with a smaller thickness did not develop primary cracks. The associated flow rule allows dilatational deformation resulting in vertical extensional primary cracks and the associated narrow troughs on the top surface. In contrast, cracks become V-shaped and grabens are associated with the primary cracks when a non-associated flow rule with a zero dilation angle is imposed. Since the temporal and spatial variations in crustal thickness reflect changes in the tectonic settings of a ridge system, the brittle deformation around the ridge system can also be attributed to tectonic origins. The larger spacing of thermally-induced brittle deformation in a thicker crust provides a qualitative explanation for the correlation between anomalously thick crust and the lack of fracture zone in the Reykjanes ridge. By the same token, the connection between thin crust and increased number of fracture zones within the AAD appears parallel to the small spacing of primary cracks in a thin crust.

Acknowledgements

We thank Joann Stock, Laetitia Le Pourhiet, and Paul Asimow for fruitful discussions and Dietmar Müller for suggestions on the manuscript. We would like to thank Claude Jaupart, Louis Geli, and two other anonymous reviewers for their useful and constructive reviews. This is contribution number 9174 of the Division of Geological and Planetary Sciences and 72 of the Tectonics Observatory. Development of SNAC was partially supported by the NSF ITR program under EAR-0205653. All calculations carried out on the Caltech Geosciences Supercomputer Facility partially supported by NSF EAR-0521699. Additional support provided through the Caltech Tectonics Observatory by the Gordon and Betty Moore Foundation.

References

Albert, R.A., Phillips, R.J., Dombard, A.J., Brown, C.D., 2000. A test of the validity of yield strength envelopes with an elastoviscoplastic finite element model. Geophys. J. Int. 140, 399–409.

Anderson, R.N., Langseth, M.G., Scalter, J.G., 1977. The mechanisms of heat transfer through the floor of the Indian Ocean. J. Geophys. Res. 82, 3391–3409.

Barnouin-Jha, K., Parmentier, E.M., Sparks, D.W., 1997. Buoyant mantle upwelling and crustal production at oceanic spreading centers: on-axis segmentation and off-axis melting. J. Geophys. Res. 102, 11979–11989.

Bathe, K.-J., 1996. Finite Element Procedure. Prentice Hall, Upper Saddle River.

Bell, R., Buck, W., 1992. Crustal control of ridge segmentation inferred from observations of the Reykjanes ridge. Nature 357, 583–586.

Bird, P., 2003. An updated digital model of plate boundaries. Geochem. Geophys. Geosyst. 4, 1027. doi:10.1029/2001GC000252.

Boley, B.A., Weiner, J.H., 1960. Theory of Thermal Stresses. John Wiley & Sons, Inc., New York.

Briais, A., Rabinowicz, M., 2002. Temporal variations of the segmentation of slow to intermediate spreading mid-ocean ridges 1. synoptic observations based on satellite altimetry data. J. Geophys. Res. 107, 2098. doi:10.1029/2001JB000533.

Bunch, A.W.H., Kennett, B.L.N., 1980. The crustal structure of the Reykjanes ridge at 59° 30′N. Geophys. J. R. Astron. Soc. 61, 141–166.

Carbotte, S.M., Small, C., Donnelly, K., 2004. The influence of ridge migration on the magmatic segmentation of mid-ocean ridges. Nature 429, 743–746.

Chen, Y., 1992. Oceanic crustal thickness versus spreading rate. Geophys. Res. Lett. 19, 753–756.

Chen, Y., Morgan, W.J., 1990a. Rift valley/no rift valley transition at mid-ocean ridges. J. Geophys. Res. 95, 17571–17581.

Chen, Y., Morgan, W.J., 1990b. A nonlinear rheology model for mid-ocean ridge axis topography. J. Geophys. Res. 95, 17583–17604.

Choblet, G., Parmentier, E.M., 2001. Mantle upwelling and melting beneath slow spreading centers: effects of variable rheology and melt productivity. Earth Planet. Sci. Lett. 183, 589–604.

Choi, E., Thoutireddy, P., Lavier, L., Quenette, S., Tan, E., Gurnis, M., Aivazis, M., Appelbe, B., in preparation. Coupling models of crustal deformation and mantle convection with a computational framework.

Chopra, P.N., Patterson, M.S., 1984. The role of water in the deformation of dunite. J. Geophys. Res. 89, 7861–7876.

Collette, B.J., 1974. Thermal contraction joints in a spreading seafloor asorigin of fracture zones. Nature 251, 299–300.

Cundall, P., 1989. Numerical experiments on localization in frictional materials. Ingenieur Arch. 58, 148–159.

de Sousza Neto, E.A., Andrade Pires, F.M., Owen, D.R.J., 2005. F-bar-based linear triangles and tetrahedral for finite strain analysis of nearly incompressible solids. Part I: formulation and benchmarking. Int. J. Numer. Methods Eng. 62, 353–383.

Dixon, J.E., Stolper, E.M., Holloway, J.R., 1995. An experimental study of water and carbon dioxide solubilities in mid-ocean ridge basaltic liquids. Part I: Calibration and solubility models. J. Petrology 36, 1607–1631.

Haxby, W.F., Parmentier, E.M., 1988. Thermal contraction and the state of stress in the oceanic lithosphere. J. Geophys. Res. 93, 6419–6429.

Hayes, D.E., Conolly, J.R., 1972. Morphology of the southeast Indian Ocean, in Antarctic Oceanography II: The Australian–New Zealand Sector. In: Hayes, D.E. (Ed.), Antarct. Res. Ser., vol. 19. AGU, Washington, D.C., pp. 125–145.

Hirth, G., 2002. Laboratory constraints on the rheology of the upper mantle. In: Karato, S., Wenk, H.-R. (Eds.), Plastic deformation of minerals and rocks, Reviews in mineralogy & geochemistry, 51. The Mineralogical Society of America, pp. 97–120.

Hirth, G., Kohlstedt, D.L., 1996. Water in the oceanic upper mantle: implications for rheology, melt extraction and the evolution of the lithosphere. Earth Planet. Sci. Lett. 144, 93–108.

Hirth, G., Escartin, J., Lin, J., 1998. The rheology of the lower oceanic crust: implications for lithospheric deformation at mid-ocean ridges. In: Buck, W.R., Delaney, P.T., Karson, J.A., Lagabrielle, Y. (Eds.), Faulting and magmatism at mid-ocean ridges. . Geophys. Monogr., vol. 106. AGU, pp. 291–303.

Jaeger, J., Cook, N., 1976. Fundamentals of rock mechanics, 2nd ed. Cahpman and Hall, London.

Karato, S., 1986. Does partial melting reduce the creep strength of the upper mantle? Nature 319.

Kastens, K.A., 1987. A compendium of causes and effects of processes at transform faults and fracture zones. Rev. Geophys. 25, 1554–1562.

Kaus, B., Podladchkov, Y., 2006. Initiation of localized shear zones in viscoelastoplastic rocks. J. Geophys. Res. 111. doi:10.1029/2005JB003652.

Kirby, S., 1983. Rheology of lithosphere. Rev. Geophys. 21, 1458–1487.

Klein, E.M., Langmuir, C.H., Staudigel, H., 1991. Geochemistry of basalts from the Southeast Indian Ridge, 115°E–138°E. J. Geophys. Res. 96, 2089–2107.

Kohlstedt, D.L., Evans, B., Mackwell, S., 1995. Strength of the lithosphere: constraints imposed by laboratory experiments. J. Geophys. Res. 100, 17587–17602.

Lachenbruch, A.H. (Ed.), 1962. Mechanics of thermal contraction cracks and ice-wedge polygons in permafrost. The Geological Society of America. Special Paper — Geological Sociery of America.

Lavier, L., Buck, W., 2002. Half graben versus large-offset low-angle normal fault; importance of keeping cool during normal faulting. J. Geophys. Res. 107. doi:10.1029/2001JB000513.

Lavier, L.L., Buck, W.R., Poliakov, A.N.B., 2000. Factors controlling normal fault offset in an ideal brittle layer. J. Geophys. Res. 105, 23431–23442.

Lin, J., Phipps Morgan, J., 1992. The spreading rate dependence of three-dimensional mid-ocean ridge gravity structure. Geophys. Res. Lett. 19, 13–16.

MacDonald, K.C., 1998. Linkages between faulting, volcanism, hydrothermal activity and segmentation of fast spreading centers. In: Buck, R.W., Delaney, P.T., Karson, J.A., Lagabrielle, Y. (Eds.), Faulting and magmatism at mid-ocean ridges. Geophys. Monogr., vol. 106. AGU, pp. 27–58.

MacDonald, K.C., Scheirer, D.S., Carbotte, S.M., 1991. Mid-ocean ridges: discontinuities, segments and giant cracks. Science 253, 986–994.

Mackwell, S., Zimmerman, M., Kohlstedt, D.L., 1998. High-temperature deformation of dry diabase with application to tectonics on Venus. J. Geophys. Res. 103.

Madge, L.S., Sparks, D.W., 1997. Three-dimensional mantle upwelling, melt generation, and melt migration beneath segment slow spreading ridges. J. Geophys. Res. 102, 20571–20583.

Marks, K., Stock, J., Quinn, J., 1999. Evolution of the australian-antarctic discordance since miocene time. J. Geophys. Res. 104, 4967–4981.

Marti, J., Cundall, P., 1982. Mixed discretization procedure for accurate modeling of plastic collapse. Int. J. Numer. Anal. Methods Geomech. 6, 129–139.

Murton, B., Parson, L., 1993. Segmentation, volcanism and deformation of oblique spreading centres: a quantative study of the reykjanes ridge. Tectonophysics 222, 237–257.

Nichols, A.R.L., Carroll, M.R., Höskuldsson, Á., 2002. Is the Iceland hot spot also wet? Evidence from the water contents of undegassed submarine and subglacial pillow basalts. Earth Planet. Sci. Lett. 202, 77–87.

Okino, K., Matsuda, K., Christie, D., Nogi, Y., Koizumi, K., 2004. Development of oceanic detachment and asymmetric spreading at the Australian-Antarctic Discordance. Geochem. Geophys. Geosyst. 5 (Q1202). doi:10.1029/2004GC000793.

Parmentier, E.M., Haxby, W.F., 1986. Thermal stresses in the oceanic lithosphere: evidence from geoid anomalies at fracture zones. J. Geophys. Res. 91, 7193–7204.
Parmentier, E.M., Phipps Morgan, J., 1990. Spreading rate dependence of three-dimensional structure in oceanic spreading centres. Nature 348, 325–328.
Poliakov, A.N.B., Hermann, H., 1994. Self-organized criticality of plastic shear bands in rocks. Geophys. Res. Lett. 21, 2143–2146.
Poliakov, A.N.B., Podladchkov, Y., Talbot, C., 1993. Initiation of salt diapirs with frictional overburdens: numerical experiments. Tectonophysics 228, 199–210.
Poliakov, A.N.B., Hermann, H., Podladchkov, Y., Roux, S., 1994. Fractal plastic shear bands. Fractals 2, 567–581.
Poliakov, A.N.B., Podladchkov, Y., Dawson, E., Talbot, C., 1996. Salt diapirism with simultaneous brittle faulting and viscous flow. Geological Society Special Publication 100, 291–302.
Quenette, S.M., Appelbe, B.F., Gurnis, M., Hodkinson, L.J., Moresi, L., Sunter, P.D., 2005. An investigation into design for performance and code maintainability in high performance computing. Anziam J. 46, C101–C116.
Regenauer-Lieb, K., Yuen, D., 2004. Positive feedback of interacting ductile faults from coupling of equation of state, rheology and thermal-mechanics. Phys. Earth Planet. Int. 142, 113–135.
Rudnicki, J., Rice, J., 1975. Conditions for the localization of deformation in pressure-sensitive dilatant materials. J. Mech. Phys. Solids 23, 371–394.
Rutter, E., 1986. On the nomenclature of model of failure transitions in rocks. Tectonophysics 122, 381–387.
Sandwell, D.T., 1986. Thermal stress and the spacings of transform faults. J. Geophys. Res. 91, 6405–6417.
Sandwell, D.T., Smith, W.H.F., 1997. Marine gravity anomaly from Geosat and ERS 1 satellite altimetry. J. Geophys. Res. 102, 10039–10054.
Sandwell, D.T., Fialko, Y., 2004. Warping and cracking of the Pacific plate by thermal contraction. J. Geophys. Res. 109. doi:10.1029/2004JB003091.
Shaw, W.J., Lin, J., 1996. Models of ocean ridge lithospheric deformation: dependence on crustal thickness, spreading rate, and segmentation. J. Geophys. Res. 101, 17977–17993.
Simo, J., Hughes, T., 2004. Computational Inelasticity. Springer.
Smallwood, J.R., White, R.S., 1998. Crustal accretion at the Reykjanes Ridge, 61°–62°N. J. Geophys. Res. 103, 5185–5201.
Tolstoy, M., Harding, A., Orcutt, J., Phipps Morgan, J., 1995. Crustal thickness at the australian-antarctic discordance and neighboring southeast Indian ridge. Eos Trans. AGU. 76, Fall Meet. Suppl., F570.
Turcotte, D.L., 1974. Are transform faults thermal contraction cracks? J. Geophys. Res. 79, 2573–2577.
Vermeer, P.A., 1990. The orientation of shear bands in biaxial tests. Géotechnique 40, 223–226.
Weissel, J.K., Hayes, D.E., 1974. The Australian-Antarctic Discordance: new results and implications. J. Geophys. Res. 79, 2579–2587.
Wessel, P., 1992. Thermal stresses and the bimodal distribution of elastic thickness estimates of the oceanic lithosphere. J. Geophys. Res. 97, 14177–14193.
White, R., McKenzie, D., O'nions, R., 1992. Oceanic crustal thickness from seismic measurements and rare earth element inversions. J. Geophys. Res. 97, 19683–19715.